Supporting Information

Highly Conjugated Poly(N-heteroacene) Nanofibers for Reversible Na storage with Ultra-High-capacity and Long cycle life

Tiantian Gu[a b], Min Zhou[a]*, Bing Huang[c], Mengyun Liu[b], Xiaolin Xiong[b], Kangli Wang[a], Shijie Cheng[a], Kai Jiang[ab]

a. State Key Laboratory of Advanced Electromagnetic Engineering and Technology School of Electrical and Electronic Engineering, Huazhong University of Science and Technology, Wuhan, Hubei 430074, China.
b. State Key Laboratory of Materials Processing, and Die & Mould Technology, School of Materials Science and Engineering, Huazhong University of Science and Technology, Wuhan, Hubei 430074, China.
c. Institute of Physical Chemistry and National Center for Computational Design and Discovery of Novel Materials (MARVEL),Department of Chemistry, University of Basel, Klingelbergstrasse 80, 4056 Basel, Switzerland.

***Corresponding author**: kjiang@hust.edu.cn, minzhou0729@hust.edu.cn

1. XRD patterns of the pristine PAN and PAN thermal treated at different temperatures for 6 h

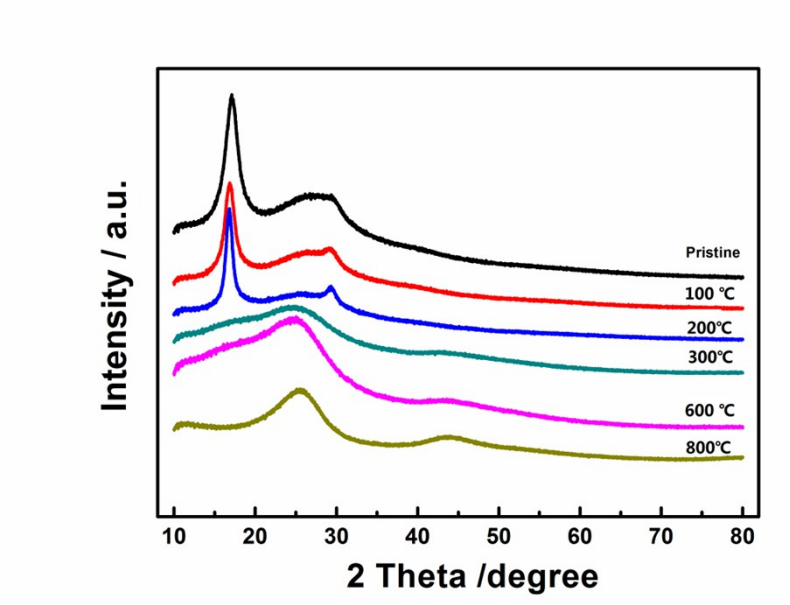

Figure S1. XRD patterns of the pristine PAN and PAN thermal treated at different temperatures (100°C - 800°C)

The products of PAN treated at different temperatures (100~800ºC) are investigated by X-ray diffraction (XRD). For the pristine PAN, the typical sharp peaks at 16.88º and 29.38º can be ascribed

to (100) and (010) diffraction, while the peak at 25.88 is speculated to the diffraction of amorphous molecular chain. When temperature increases to 300ºC, the peaks at 25.88º and 29.38º disappear. When further increasing to 800 ºC, the peak at 16.88 disappears. Two sharp peaks at 25.18 and 43.68 assigned to (002) and (10) diffraction of pseudo-graphite appear, implying the deposition of the organic polymer structure and carbonization.

2. **Raman spectrum**

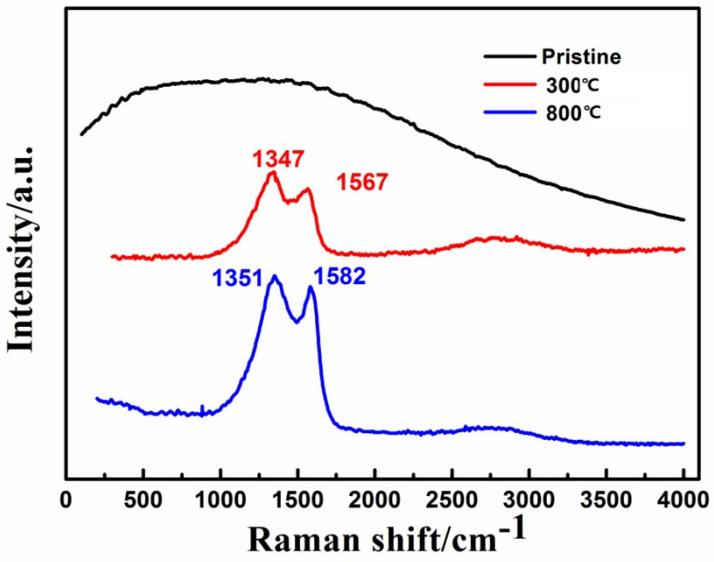

Figure S2. Raman spectrum of the pristine PAN and PAN treated at 300 °C and 800 °C

The pristine PAN shows a strong fluorescence in Raman spectrum. When treated at 300°C，two bands centered at 1347 cm^{-1} and 1567 cm^{-1} corresponding to the D and G-band. In general, the D band is attributed to defects and disorder in the hexagonal graphitic layers, while the G band is ascribed to the vibration of sp^2 carbon atoms in a 2D hexagonal lattice. As the temperature increase to 800 ℃, the I_D/I_G value decreases from 1.14 to 1.06, indicating higher orientation and higher graphitic order.

3. **FT-IR spectrum of the pristine PAN and PAN thermal treated at different temperatures**

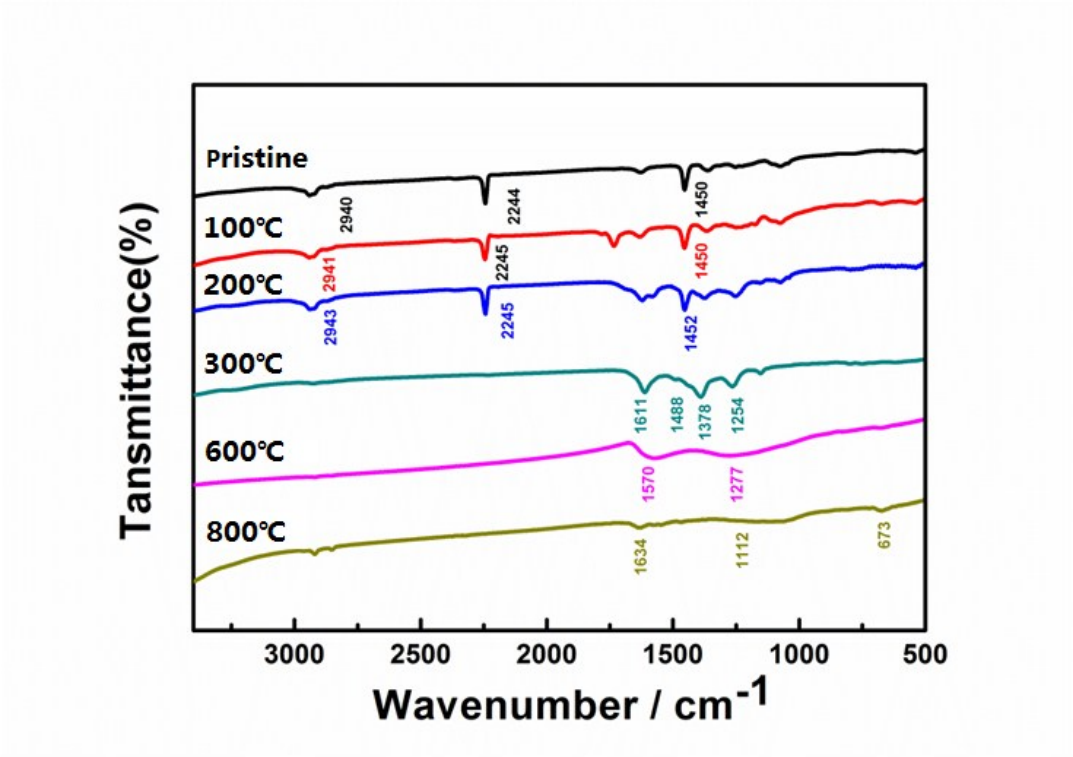

Figure S3. FT-IR spectrum of the pristine PAN and PAN thermal treated at different temperatures (100°C - 800°C)

For the pristine PAN, the single peak at 2240 cm^{-1} should be ascribed to the typical absorption of C≡N groups. For the sample treated at 300ºC, the C≡N bands disappear and the broad absorption band around 1611 cm^{-1} should be ascribed to the absorption of mixed double bonds [C=C and C=N], implying the cyclization of cyano-group (C≡N) and generation of heterocyclic ring (C=N and C=C groups). As the temperature gets higher, the poly(heteroacene) structure transform to N-doped carbon fibers.

4. **FT-IR spectrum of the polyacene (PAc) and cPAN.**

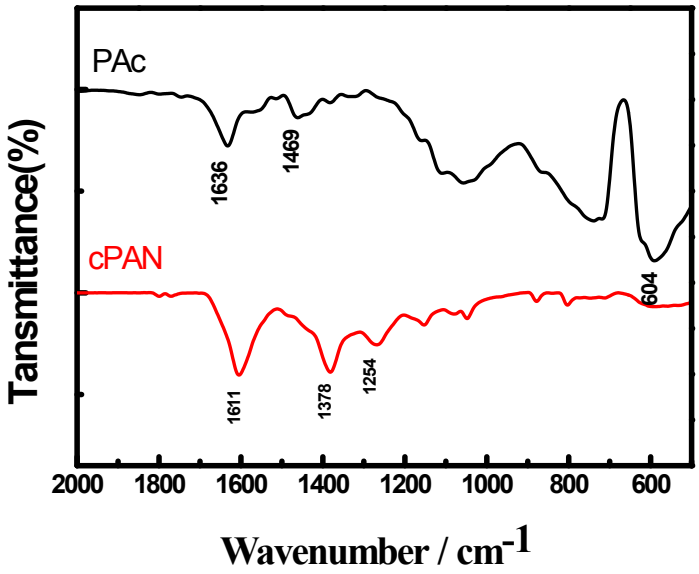

Figure S4. FT-IR spectrum of the PAc and cPAN

For the polyacene, the peaks in the region of 1400 - 1600cm^{-1} are corresponding to the conjugated vibration, and the peak at 604 cm^{-1} belongs to the aromatic ring.

5. Thermogravmetric analysis (TGA)

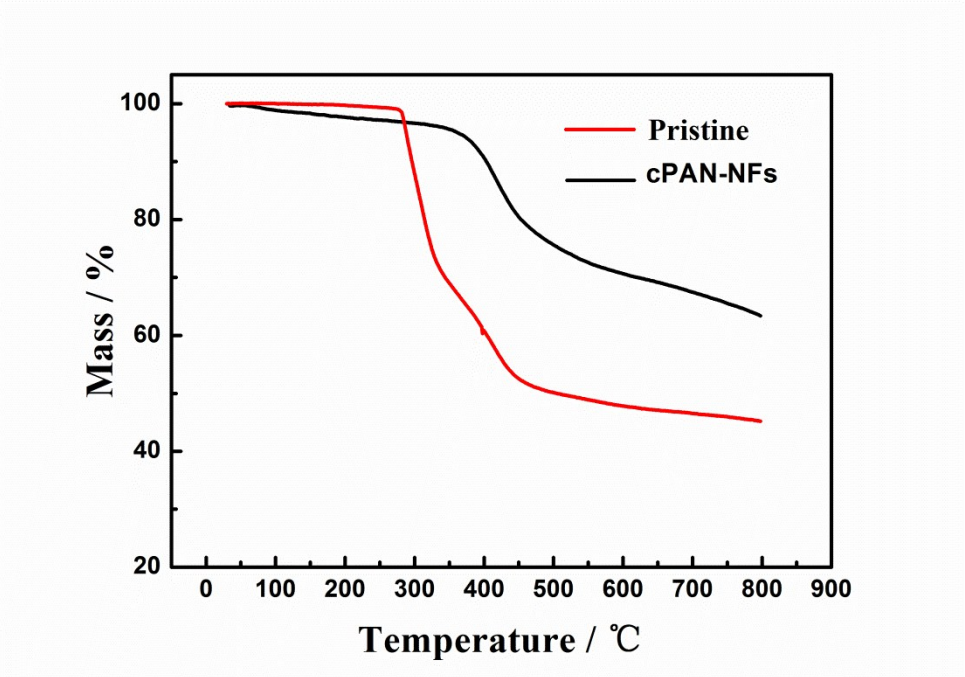

Figure S5. TG curves of pristine PAN and as-prepared cPAN-NFs

The TG curve of pristine PAN exhibits two main stages of weight loss. The first occur in the temperature range of 250–300°C, which could be ascribed to the cyclization process of PAN with little weight loss. The great weight loss of pristine PAN in the temperature range of 280–450°C, which corresponds to the carbonization with the emission of H, C, N and oligomers. [1]

6. ^{13}C solid-state NMR spectrum

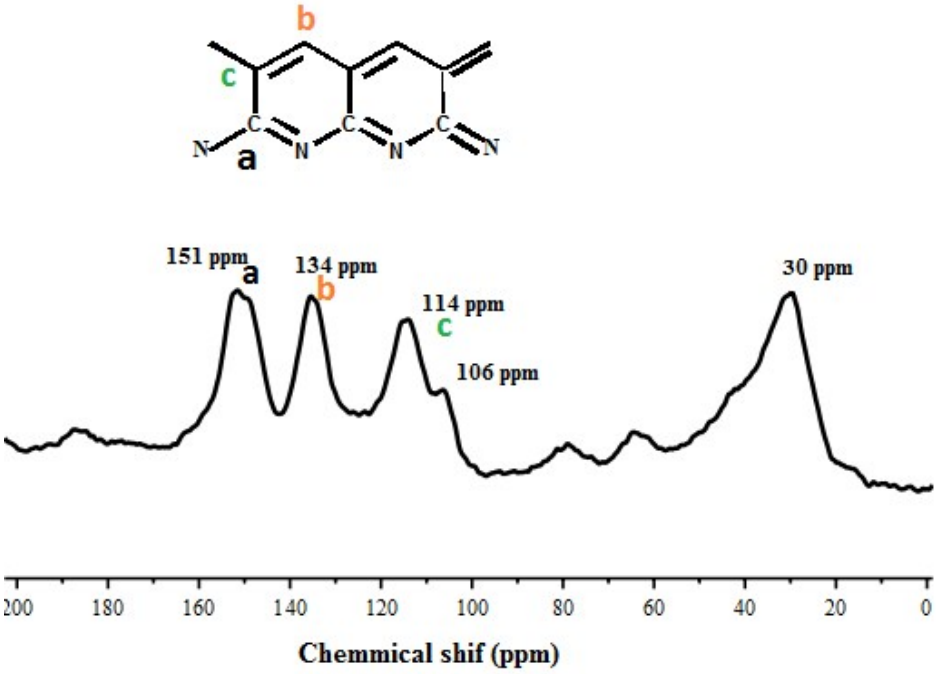

Figure S6. The ^{13}C solid state DP/MAS NMR spectra of cPAN-NFs

7. XPS characterization of cPAN

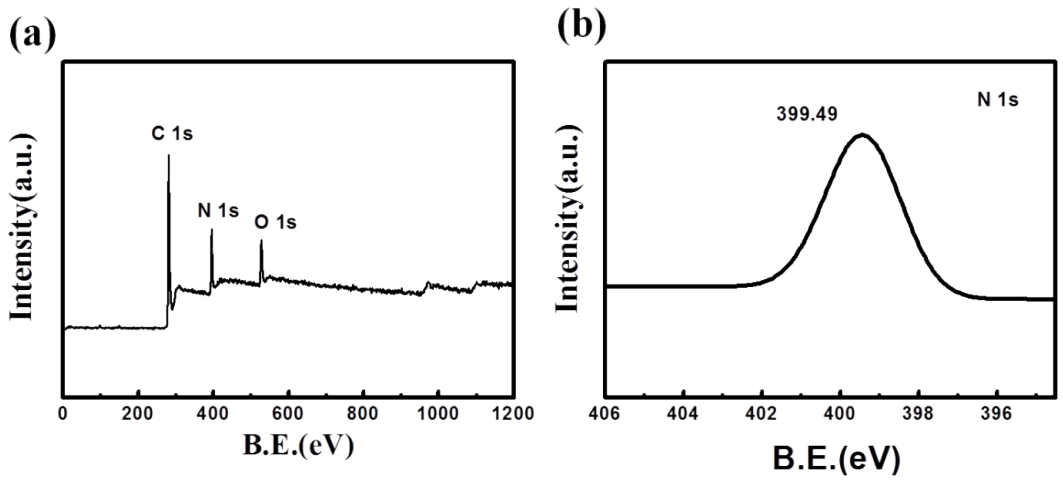

Figure S7. (a) X-ray photoelectron spectra of the as-prepared cPAN, (b) high resolution image of N1s bands

The binding energy for N 1s electrons appeared at 399.49 eV which is attributed to the aromatic nitrogen, indicating that the nitrogen incorporation into the polyacene backbone.

8. Elemental composition of the pristine PAN, as-prepared cPAN-NFs

Table S1. Elemental composition information of pristine PAN and cPAN-NFs

Sample	C(wt%)	N(wt%)	H(wt%)
Pristine PAN	67.92	26.42	5.660
cPAN-NFs	65.67	22.23	4.462

9. **The morphology characteristics of the as-prepared PAc, cPAN-PANs and bulk cPAN**

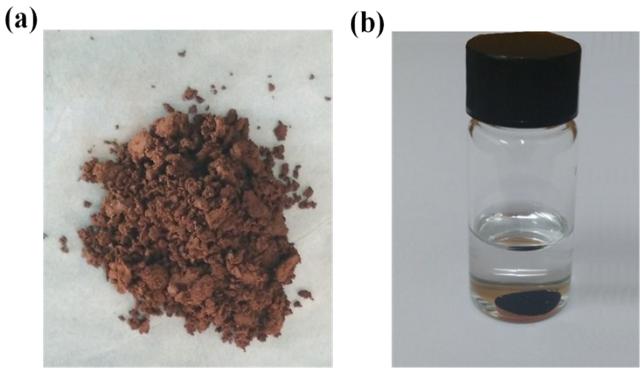

Figure S8. Digital image of (a) cPAN-NFs powders (b) cPAN-NFs electrode steeped in $NaPF_6$/DME after 36 h

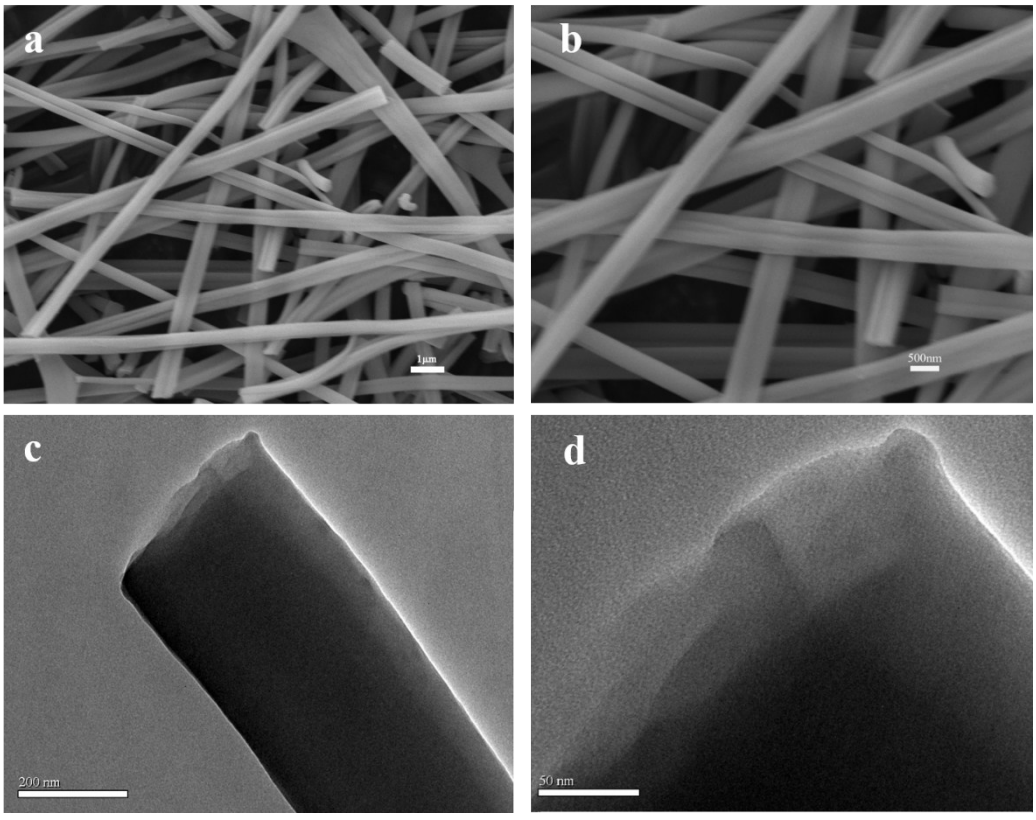

Figure S9. SEM image of the as-prepared cPAN-NFs (a) and (b); TEM image of the as-prepared cPAN-NFs (c) and (d).

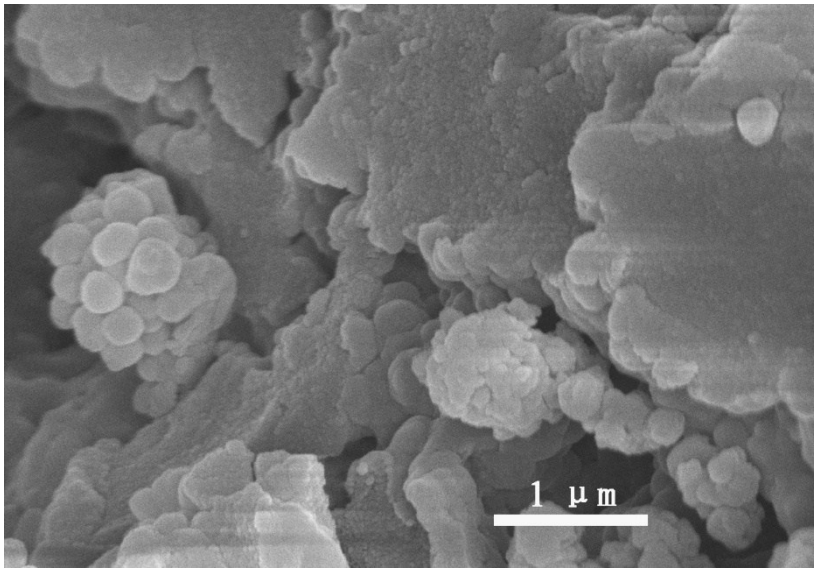

Figure S10. SEM image of the bulk cPAN

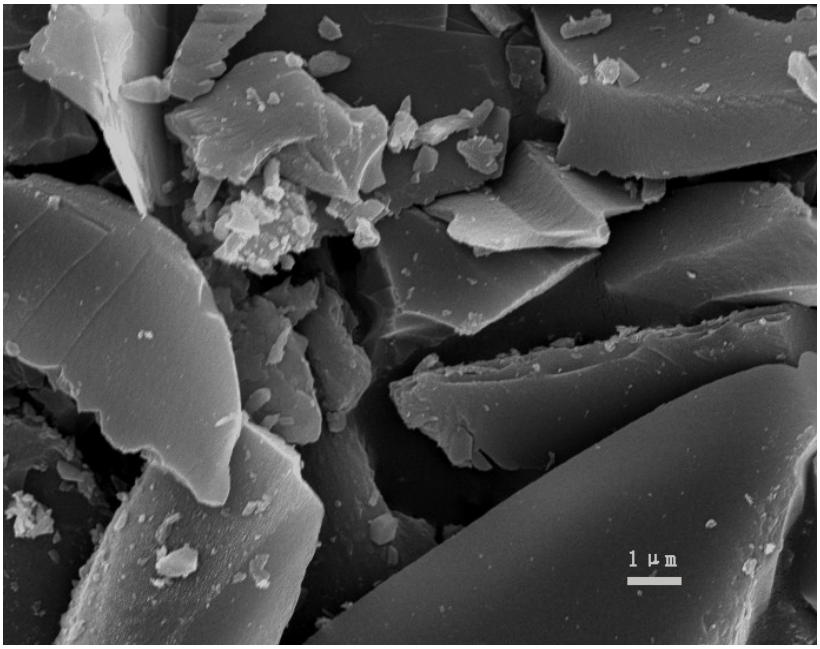

Figure S11. SEM image of the polyacene

For comparison, polyacene (PAc) show a flake-like architecture with particle size of ~10 um.

10. **Nitrogen adsorption/desorption isotherms of the as-prepared cPAN-NFs**

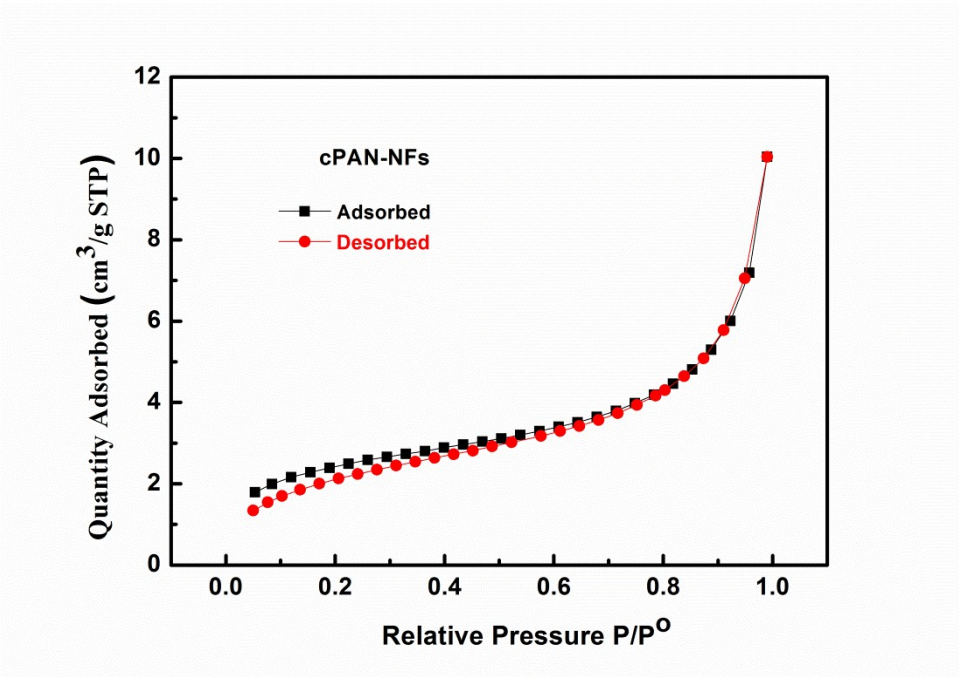

Figure S12. Nitrogen adsorption/desorption isotherms of as-prepared cPAN-NFs

11. The electronic structure of cPAN and other conventional conducting polymers (PAc, PANI, PPy, PTh)

Table S2. Elemental composition information of PAN and cPAN-NFs

Polymer	cPAN	PAc	PANI	PPy	PTh
HOMO(eV)	-5.44	-4.08	-3.96	-4.04	-4.66
LUMO (eV)	-4.65	-3.02	-0.23	-0.85	-2.93
E_g**(eV)** (HOMO-LUMO gaps)	**0.79**	**1.06**	**3.73**	**3.19**	**1.73**

12. **Charge-discharge profiles of the PAN treated at 300 °C for different time.**

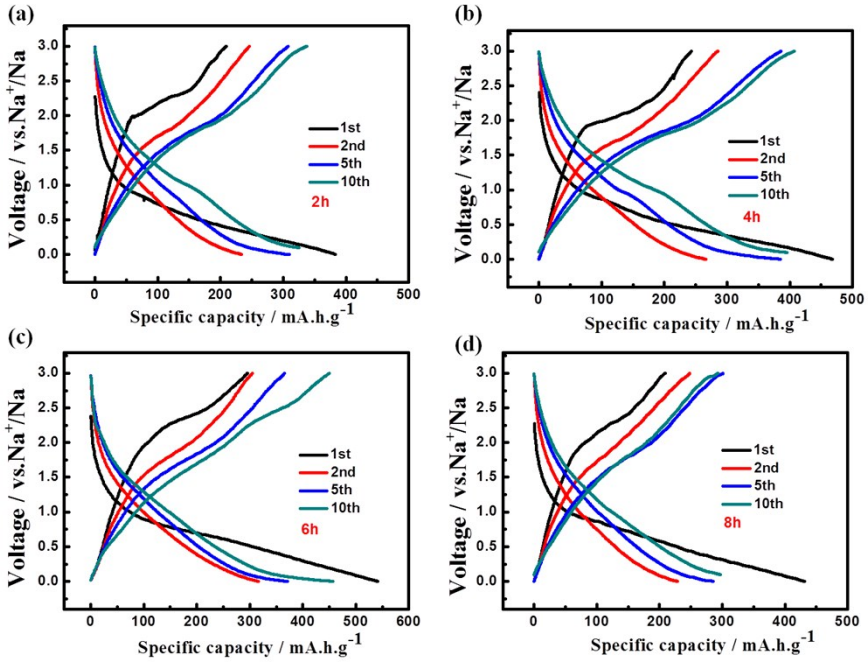

Figure S13. Charge-discharge profiles of cPAN-NFs electrode thermal treated at 300 °C for (a) 2 h; (b) 4 h; (c) 6 h; (d) 8 h in $NaPF_6$/DME in the voltage range of from 0.001 to 3 V. Current density: 50 mA g^{-1}

To evaluate the effect of thermal treating time on the electrochemical performances of cPAN-NFs, the Na-storage performance of the cPAN-NF thermal treated at 300 °C for various periods of time is measured. As shown in Figure S14, the cPAN-NFs electrode deliver reversible capacities of 320, 400, 450 and 300 mA h g^{-1} for the samples treated for 2, 4, 6, 8 h, respectively.

The cPAN-NFs samples treated for 6 h exhibit the best Na-storage performances due to the well-formed pseudo-graphite microstructure. Extending the heating time is beneficial to generate conjugated planes with high conjugated extent and large size of pseudo-graphite crystal [2-6].

13. **Electrochemical performances of the carbon addictive (KB and MWCNT)**

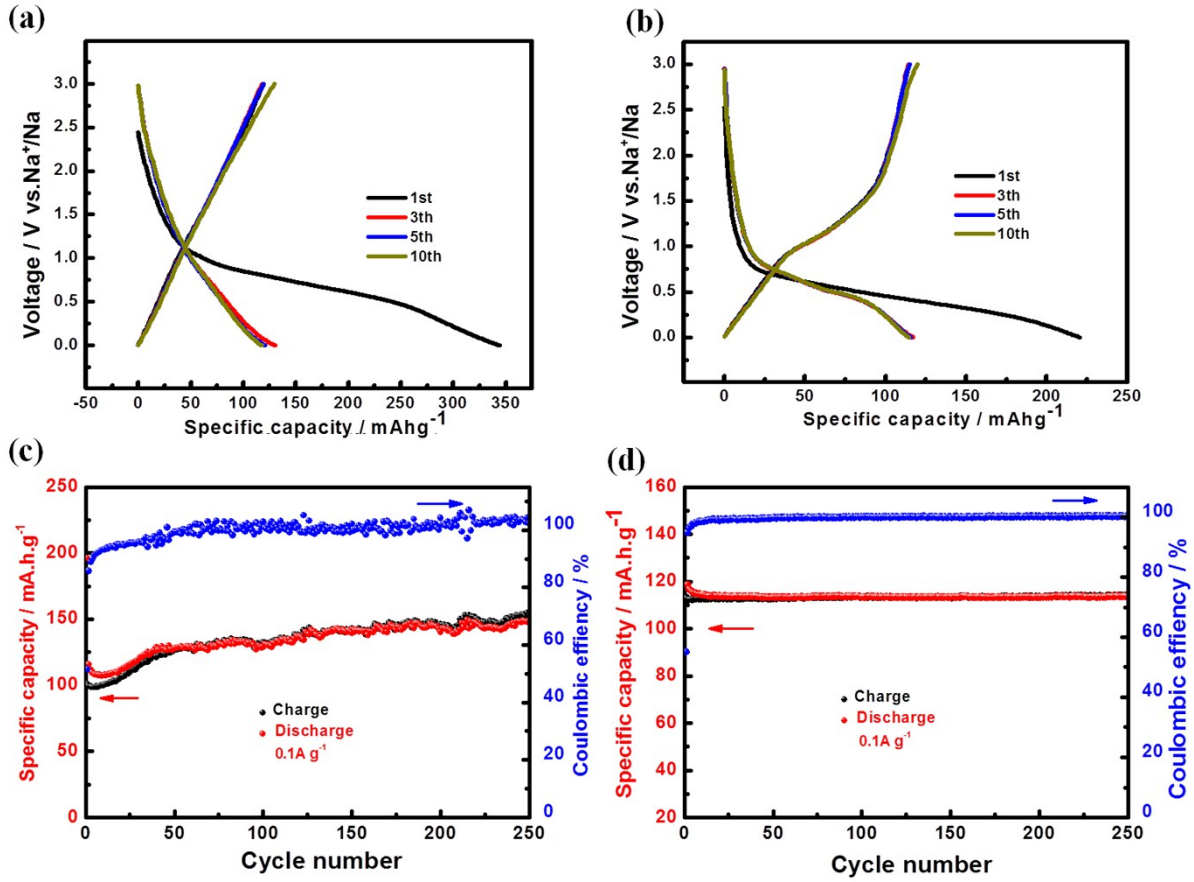

Figure S14. The charge-discharge profiles of Ketchen black (a) and MWCNT (b) at 0.05A g^{-1}; Cycling performance of Ketchen black (c) and MWCNT (d) in 1.0 mol L^{-1} $NaPF_6$/DME at 0.1 A g^{-1}.

As shown in Figure S15, the carbon addictive KB and MWCNT can deliver a reversible capacity of 130, 115 mA h g^{-1}, respectively. As the weight ratio of cPAN/KB/MWCNT = 6/2/1, the capacities contribution of KB and MWCNT are 26 and 11.5 mA h g^{-1}, which are negligible compared to the high capacity of cPAN (527 mA h g^{-1}).

14. **Na storage performances of the bulk cPAN electrode**

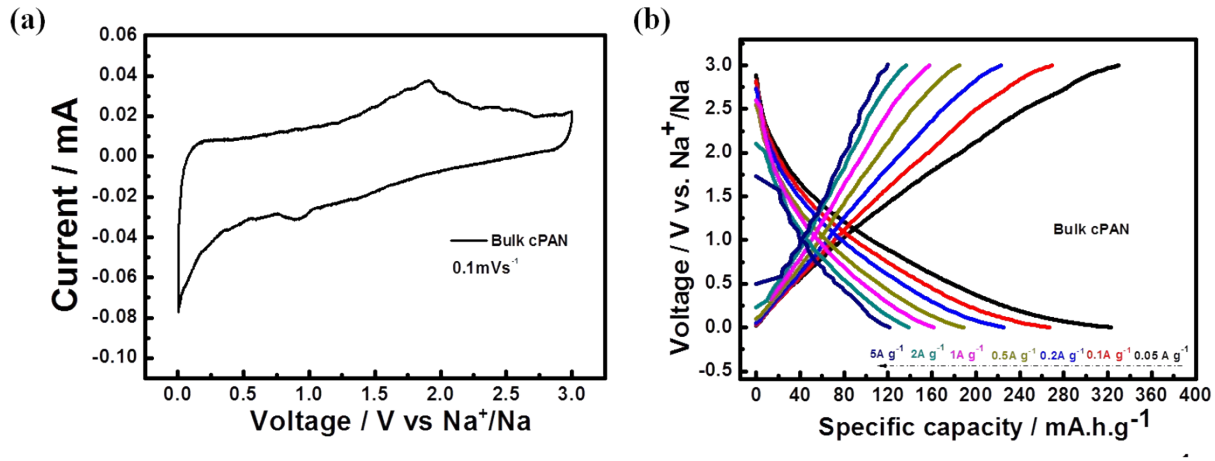

Figure S15. Na storage performance of the bulk cPAN electrode in $NaPF_6$/DME in the voltage range of from 0.001 to 3 V: (a) Cyclic voltammetry curves scanned at a rate of 0.1 mVs^{-1} (b) charge-discharge profiles at different current densities.

15. Capacity retention and charge-discharge profiles of cPAN-NFs at $5Ag^{-1}$

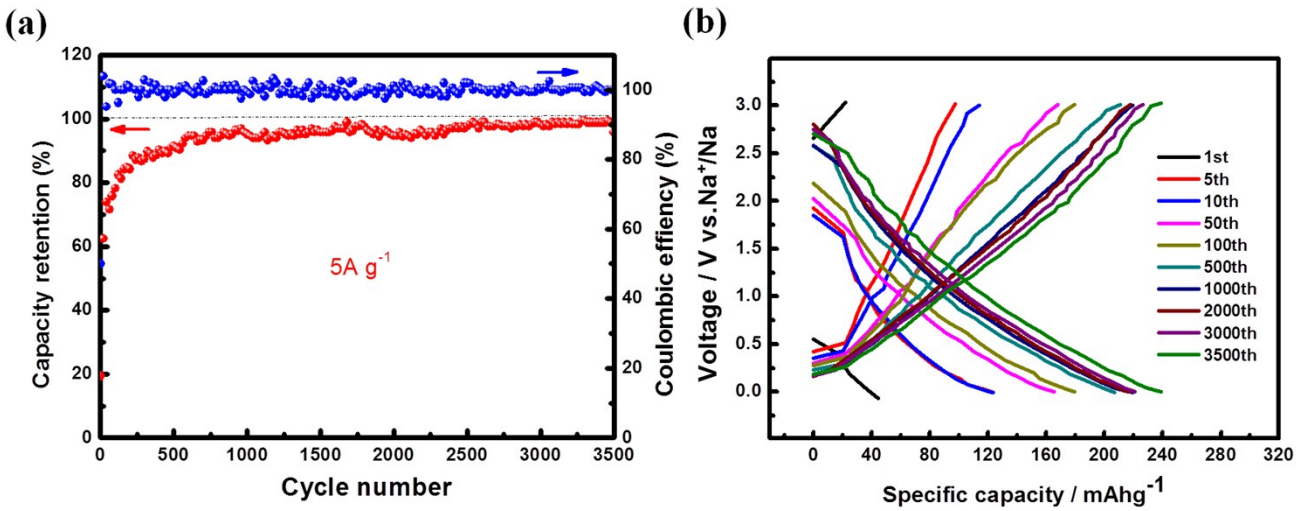

Figure S16. Capacity retention (a) and charge-discharge profiles (b) of cPAN-NFs at $5Ag^{-1}$.

As shown in Fig 3c and FigS19 a, the discharge and charge capacities of the PAN-NFs in the first cycle are 44.4 and 22.2 mA h g^{-1}, corresponding to an initial columbic efficiency of 50%. Then the

capacity increased up to 200 mA h g^{-1} and came to be stable. After 3500 cycles, a capacity retention of 99.4% could be obtained with stable coulombic efficiency up to 99.9%. As shown in FigS19 b, the charge/discharge curves exhibit no obvious change except for the lower polarization.

16. Comparison of the Na –storage performances of cPAN-NFs in this study with other Na-storage anode materials previously reported in the literature

Table S3. Comparison of Na storage performances of cPAN-NFs with other organic anode materials

Anode	Capacity/Current density	Cycle number/capacity retention	Reference
cPAN-NFs	527 mA h g^{-1}/0.1 A g^{-1} 195.7 mA h g^{-1}/5 A g^{-1}	3500/~100%	This work
Na_2TP	295 mA h g^{-1}/0.03 A g^{-1} 100 mA h g^{-1}/3 A g^{-1}	90/90%	[7]
Na_2bpdc	200 mA h g^{-1}/0.04A g^{-1} 100 mA h g^{-1}/3.74 A g^{-1}	150/90%	[8]
$Na_2C_6H_2O_4$/CNT	259 mA h g^{-1}/0.029A g^{-1} 142 mA h g^{-1}/2.03 A g^{-1}	30/92%	[9]
Juglone/RGO	280 mA h g^{-1}/0.1 A g^{-1} 210 mA h g^{-1}/0.4A g^{-1}	100/91.8%	[10]
SSDC	222 mA h g^{-1}/0.05 A g^{-1} 72mA h g^{-1} / 10A g^{-1}	400/70%	[11]
O-PDA-2	508 mA h g^{-1}/0.05A g^{-1} 122 mA h g^{-1}/3.2A g^{-1}	1024/~ 100%	[12]
Na_2NC/G	207 mA h g^{-1}/0.02Ag^{-1} 88 mA h g^{-1}/2 A g^{-1}	100/92%	[13]
Na_2PDC	270 mA h g^{-1}/0.015Ag^{-1} 135 mA h g^{-1}/1.57Ag^{-1}	100/83%	[14]

Table S4. Comparison of Na storage performances of cPAN-NFs with other carbon-based materials

Anode	Capacity/Current density	Cycle number/capacity retention	Reference
cPAN-NFs	527 mA h g^{-1}/0.05 A g^{-1} 195.7 mA h g^{-1}/5 A g^{-1}	3500/~100%	This work
DC-S	561 mA h g^{-1}/0.02 A g^{-1} 275 mA h g^{-1}/1 A g^{-1}	1000/85.9%	[15]
3D PCFs	356.1 mA h g^{-1}/0.1A g^{-1} 187.6 mA h g^{-1}/2.5 A g^{-1}	5000/80%	[16]
3D OC-500	483 mA h g^{-1}/0.1Ag^{-1} 299 mA h g^{-1}/1 A g^{-1}	1200/81.4%	[17]
BN-CNFs	691 mA h g^{-1}/0.1A g^{-1} 314 mA h g^{-1}/10A g^{-1}	1000/84.1%	[18]
P-CNSs	321 mA h g^{-1}/0.1A g^{-1} 149mA h g^{-1}/5A g^{-1}	5000/ nearly 100%	[19]
G/C	432.3 mA h g^{-1}/0.1A g^{-1} 330 mA h g^{-1}/2A g^{-1}	1000/94.691%	[20]

17. **Structure and morphology changes of pristine electrodes and electrodes cycled after 1700 cycles.**

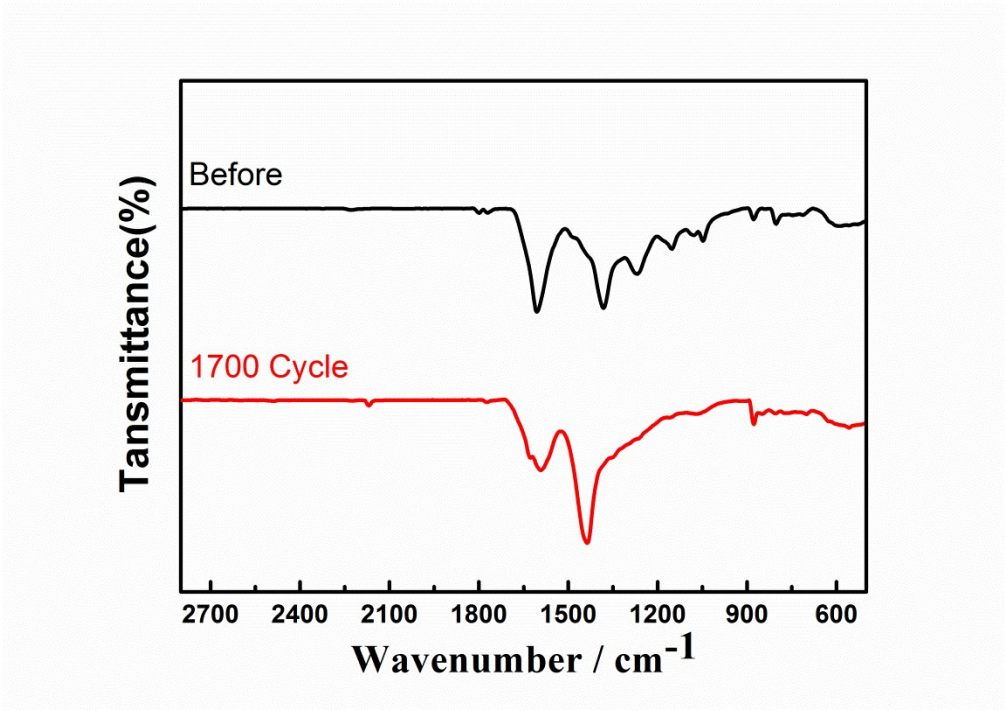

Figure S17. FT-IR spectrum of the pristine and cycled electrodes (after 1700 cycles) at 5 A g^{-1}

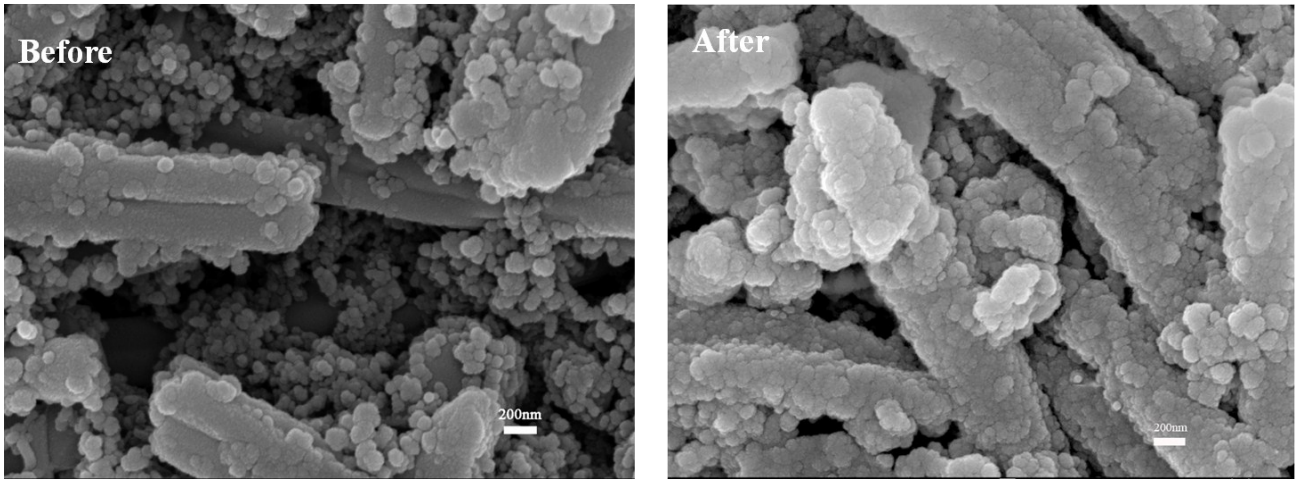

Figure S18. SEM images of the pristine and cycled electrodes (after 1700 cycles) at 5 A g^{-1}

18. Geometries and frontier molecular orbitals.

DFT calculations were done using Gaussian 09 package at the computational level of B3LYP/6-31G(D) with PCM solvation model.

The polymer system is simplified and modeled by oligomer containing 12 units (C_3NH)

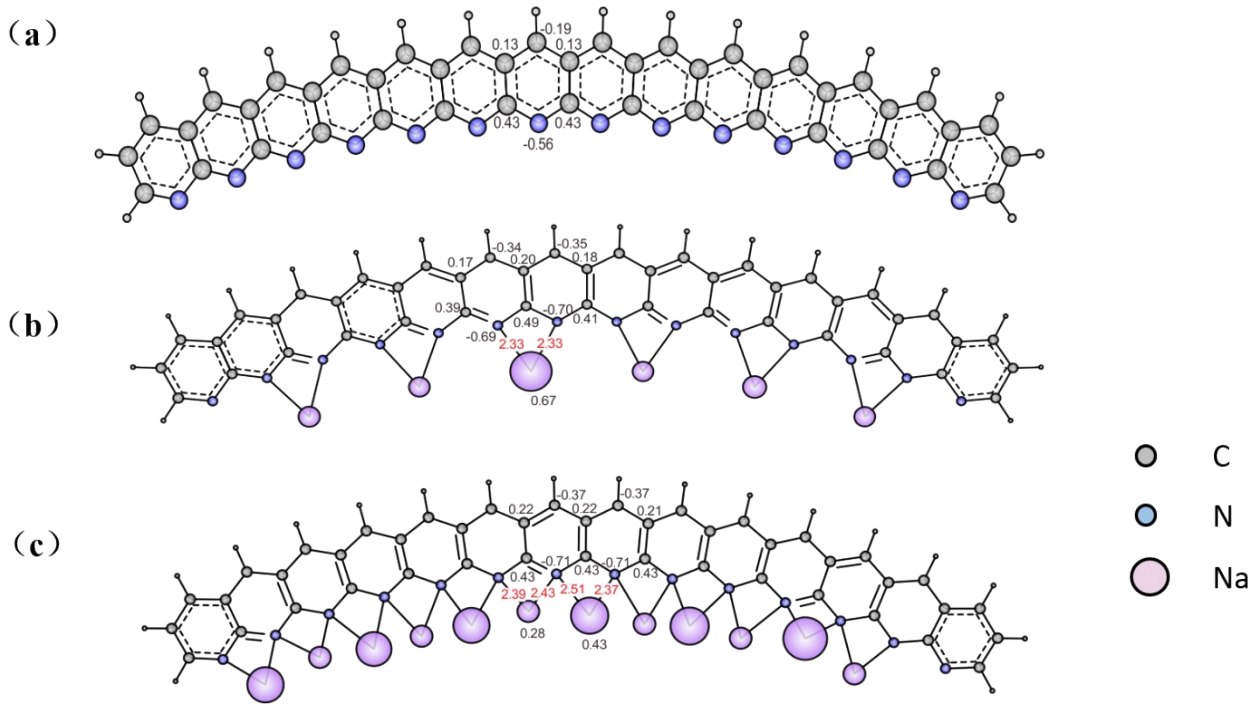

Figure S19. Mulliken charge distribution of (a) cPAN; (b) cPAN-50%Na; (c) cPAN-Na.

Red font: bond distance; Black font: Mulliken charge

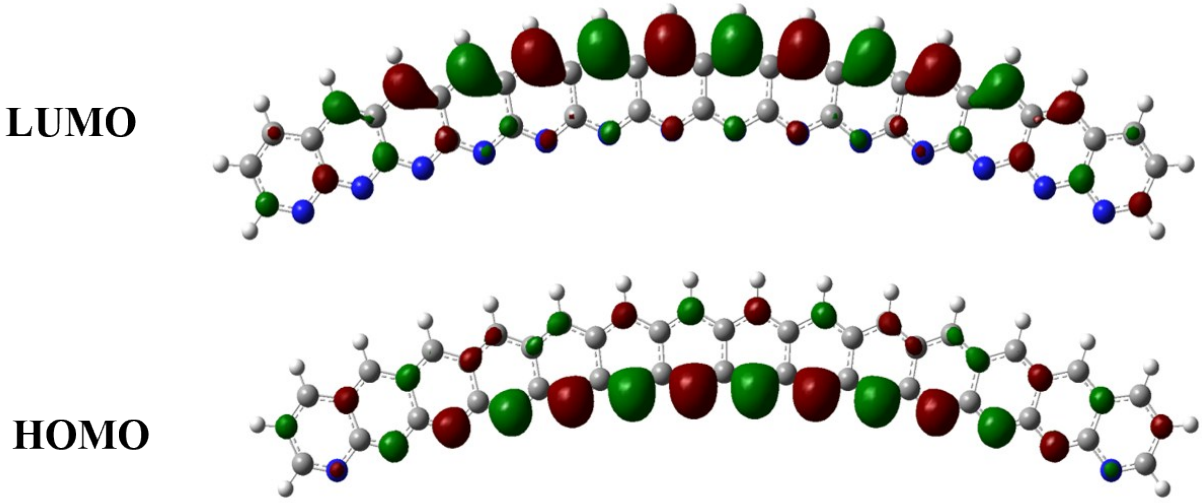

Figure S20. Frontier orbital wavefunctions of **cPAN** in Diethylether with isovalue of 0.02.

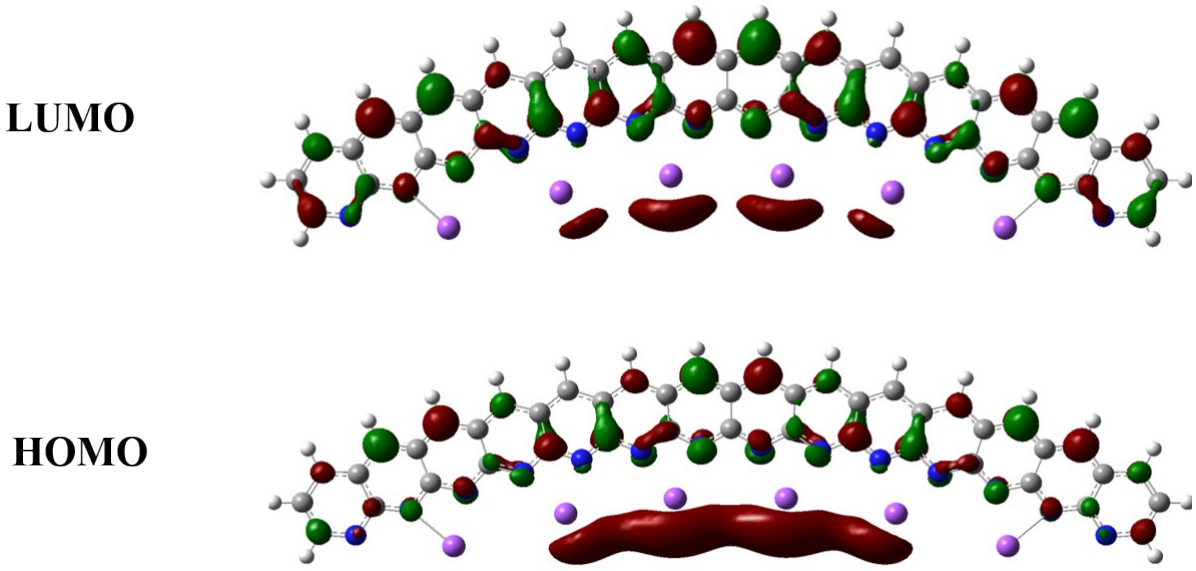

Figure S21. Frontier orbital wavefunctions of **cPAN-50%Na** in Diethylether with isovalue of 0.02.

LUMO

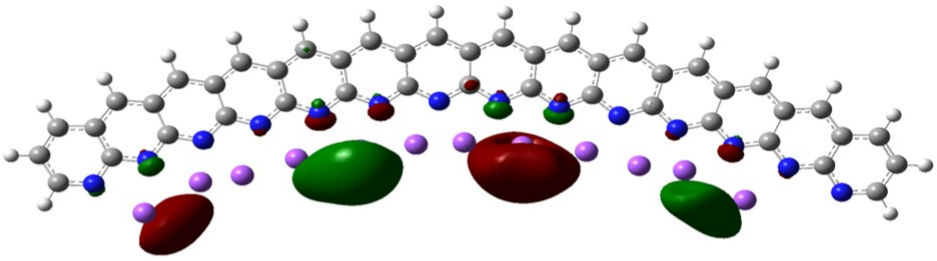

HOMO

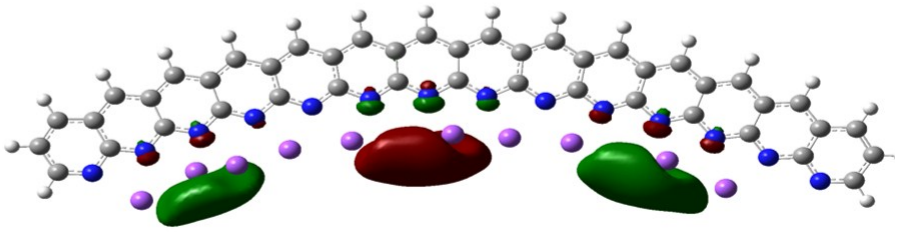

Figure S22. Frontier orbital wavefunctions of **cPAN-Na** in Diethylether with isovalue of 0.02.

Table S5. Sum of electronic and zero-point energies of the optimized structures **Na, cPAN, cPAN-50%Na, cPAN-Na**

Energy	Hartree	eV
Na	-162.2862551	
cPAN（*with 12 units*）	-2454.0680976	
cPAN-50%Na ***（12 units， 6 Na ）***	-3428.400376	
cPAN-Na ***（12 units， 12 Na ）***	-4402.2399948	
ΔE_1 （*for the first stage of Na doping*）	**-0.1024583**	**-2.7868667**
ΔE_2 （*for the second stage of Na doping*）	**-0.0203483**	**-0.5534747**

The polymer system is simplified and modeled by oligomer containing 12 units of C_3NH.

At the first stage of Na-doping (from neutral state to a doping level of 50%), 6 Na coordinate with the 12 aromatic nitrogen.

ΔE_1 =[*E (cPAN-50%Na)* -6 *E (Na)* - *E (cPAN)*]/6

At the second stage of Na-doping (from doping level of 50% to fully doped), another 6 Na insert into the polymer system

ΔE_2 =[*E (cPAN-Na)*- 6 *E (Na)* - *E (cPAN-50%Na)*]/6

Supplementary References

1. H. Wang, S. Kim, S. Cho, G. B, H. Choi, Mater. Resear. Bull. 2018, **97**, 49-55.
2. S. Lei, W. Cao, Z. Fu and L. Xu, J. Appl. Polym. Sci., 2016, **133**, 1–7.
3. S. Dalton, F. Heatley and P. M. Budd, Polymer., 1999, **40**, 5531–5543.
4. M. S. A. Rahaman, A. F. Ismail and A. Mustafa, Polym. Degrad. Stab., 2007, **92**, 1421–1432.
5. Y. Xue, J. Liu and J. Liang, J. Appl. Polym. Sci., 2013, **127**, 237–245.
6. W. X. Zhang, Y. Z. Wang and C. F. Sun, J. Polym. Res., 2007, **14**, 467–474.
7. Y. Park, D. S. Shin, S. H. Woo, N. S. Choi, K. H. Shin, S. M. Oh, K. T. Lee, S. Y. Hong, Adv. Mater.2012, **24**, 3562-7.
8. A. Choi, Y. K. Kim, T. K. Kim, M.-S. Kwon, K. T. Lee, H. R. Moon, J. Mater. Chem. A 2014, **2**, 14986-14993.
9. X. Wu, J. Ma, Q. Ma, S. Xu, Y.-S. Hu, Y. Sun, H. Li, L. Chen, X. Huang, J. Mater. Chem. A 2015, **3**, 13193-13197.
10.H. Wang, P. Hu, J. Yang, G. Gong, L. Guo, X. Chen, Adv. Mater. 2015, **27**, 2348-54.
11.C. Wang, Y. Xu, Y. Fang, M. Zhou, L. Liang, S. Singh, H. Zhao, A. Schober, Y. Lei, J. Am. Chem. Soc. 2015, **137**, 3124-30.
12.T. Sun, Z. Li, H. Wang, D. Bao, F. Meng, X. Zhang, Angew. Chem. Int. Ed. 2016, **55**, 10662-10666.
13.W. Deng, J. Qian, Y. Cao, X. Ai, H. Yang, Small 2016, **12**, 583-7.
14.H. Padhy, Y. Chen, J. Lüder, S. R. Gajella, S. Manzhos, P. Balaya, Adv. Energy Mater. 2017, 1701572.
15. W. Li, M. Zhou, H. Li, K. Wang, S. Cheng, K. Jiang, Energy Environ. Sci. 2015, **8**, 2916-2921.
16. H. Hou, C. E. Banks, M. Jing, Y. Zhang, X. Ji, Adv. Mater. 2015, **27**, 7861-6.
17. L. Fan, B. Lu, Small 2016, **12**, 2783-91.
18. M. Wang, Y. Yang, Z.Yang, L. Gu, Q. Chen, Y. Yu, Adv. Sci. 2017, **4**, 1600468.
19. H. Hou, L. Shao, Y. Zhang, G. Zou, J. Chen, X. Ji, Adv. Sci. 2017, **4**, 1600243.
20. Y. Liu, L.-Z. Fan, L. Jiao, J. Mater. Chem. A 2017, **5**, 1698-1705.